Effect of Dimerization on the Dynamics of Neurotransmitter:Sodium Symporters

Mert Gur,*,[†,‡] Mary Hongying Cheng,[†] Elia Zomot,[§] and Ivet Bahar*,[†]

[†]Department of Computational and Systems Biology, School of Medicine, University of Pittsburgh, Pittsburgh, Pennsylvania 15260, United States

[‡]Department of Mechanical Engineering, Istanbul Technical University (ITU), Istanbul 34437, Turkey

[§]Department of Biomolecular Sciences, Weizmann Institute of Science, Rehovot 7610001, Israel

S Supporting Information

ABSTRACT: Dimerization is a common feature among the members of the neurotransmitter:sodium symporter (NSS) family of membrane proteins. Yet, the effect of dimerization on the mechanism of action of NSS members is not fully understood. In this study, we examined the collective dynamics of two members of the family, leucine transporter (LeuT) and dopamine transporter (DAT), to assess the significance of dimerization in modulating the functional motions of the monomers. We used to this aim the anisotropic network model (ANM), an efficient and robust method for modeling the intrinsic motions of proteins and their complexes. Transporters belonging to the NSS family are known to alternate between outward-facing (OF) and inward-facing (IF) states, which enables the uptake and release of their substrate (neurotransmitter) respectively, as the substrate is transported from the exterior to the interior of the cell. In both LeuT and DAT, dimerization is found to alter the collective motions intrinsically accessible to the individual monomers in favor of the functional transitions (OF ↔ IF), suggesting that dimerization may play a role in facilitating transport.
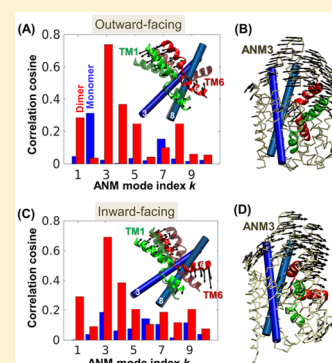
INTRODUCTION

Communication between neurons is established by neurotransmitters. Once a signal in the form of an electric current arrives to the axon terminal of the presynaptic neuron, it is chemically transmitted to the postsynaptic neuron by calcium-dependent release of neurotransmitters into the synaptic gap. Ligand-gated ion channels and G-protein-coupled receptors on the postsynaptic neuronal dendrites are activated upon binding these signaling molecules. Activation of these proteins generates excitatory or inhibitory responses in the postsynaptic cell.[1] The neurotransmitter:sodium symporter (NSS) family of transporters regulate neurotransmission by uptake (or reuptake) of excess neurotransmitters into neighboring glial cells (or the presynaptic cell).[2,3] The transport of neurotransmitters into the intracellular (IC) region against their concentration gradient is assisted by the cotransport of Na+ ions down their electrochemical gradient across the membrane—hence the name secondary transporters or symporters.[4] Control of synaptic levels of neurotransmitters is essential to avoiding several neurological disorders and cytotoxicity. NSS dysfunctions have been linked to epilepsy,[5] depression,[6,7] anxiety,[8,9] attention-deficit hyperactivity disorder (ADHD),[10] and Parkinson's disease,[7] and they serve as targets for a wide range of therapeutic or illicit drugs.

The first crystallographically resolved transporter providing structural information on the NSS family was a bacterial homologue, sodium:leucine transporter (LeuT). LeuT transports leucine and other small amino acids, such as alanine, across the bacterial cell membrane. Its structure, known as the "LeuT fold" is composed of 12 transmembrane (TM) helices organized in two inverted 5-helix repeats, TM1−5 and TM6−10.[11] The α-helical geometries of TM1 and TM6 are disrupted halfway across the membrane bilayer, thus providing binding sites for the substrate (Leu, Ala, or other amino acids) and Na+ ions. The transporter visits several states during the transport cycle, which permits it to bind, translocate, and release the substrate and ions from the extracellular (EC) to the IC region. The originally resolved LeuT structure was in an outward-facing (OF), substrate-bound, closed/occluded (OFc) state,[11] which means that the TM helices form an EC-facing vestibule while the EC gate-forming residues occlude/close the gate to prevent the escape of substrate/ions back to the EC region. In subsequent years, LeuT has been resolved in other states as well, including a substrate-free outward-facing open (OFo) state with bound Na+,[12] and without Na+ prior to uptake of substrate/Na+,[13] and substrate/Na+-free inward-facing (IF) open (IFo)[12] states, providing plenty of structural data for modeling the structure and dynamics of LeuT and mammalian homologues in NSS family.
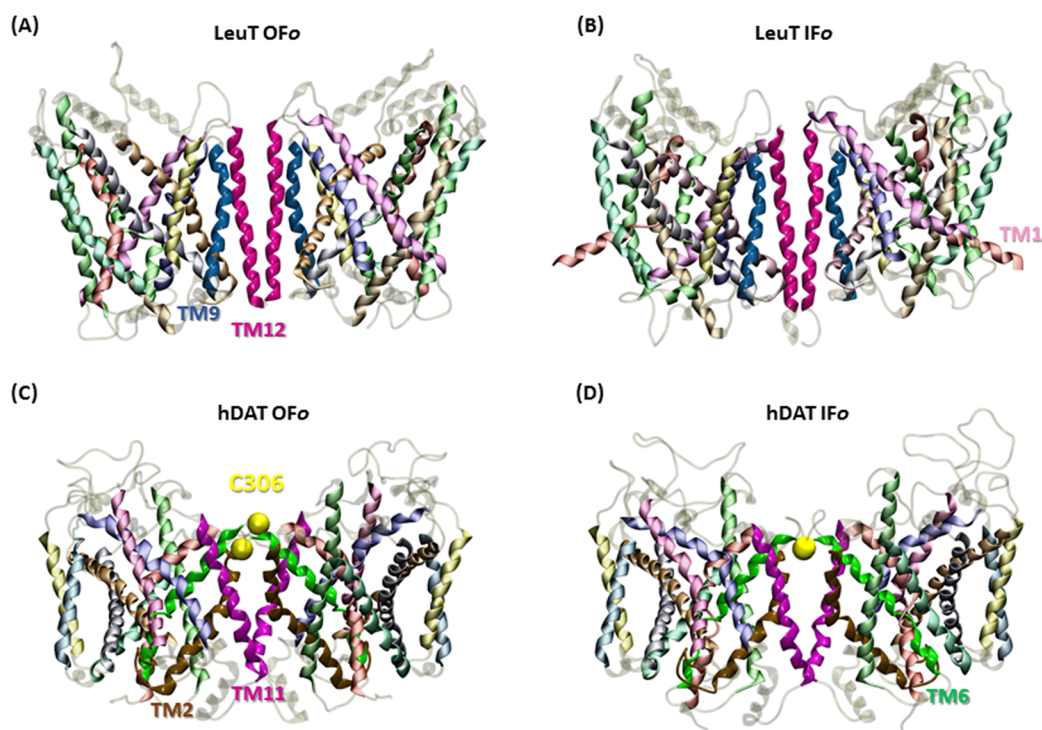
Figure 1. LeuT and hDAT dimers. The ribbon diagrams display the conformers for OFo (A) and IFo (B) LeuT dimer and OFo (C) and IFo (D) hDAT dimer used for ANM analysis. The LeuT dimeric interface involves contacts between TM9 and TM12; the hDAT dimer interface involves contacts between TM2, TM6, and TM11. TM1 and TM6 (labeled) show significant reorientation between the OF and IF states. Cys306 on both protomers are shown by yellow beads. Diagrams are generated using VMD,[66] using B-spline style for visual clarity.

The OF and IF states are global conformational properties defined by the overall packing of the TM helices; the substrate-binding pocket faces the EC or IC region, in these respective states; and open and closed refer to the local conformation of residues that serve as EC or IC gates for controlling the entry or exit of the cargo in either OF or IF states. Comparison of the crystallographically resolved OFo and IFo states of LeuT shows reorientations in TM1 and TM6 (Figures 1 and 2), accompanied by cooperative rearrangements in TM helices. In addition to structural information obtained from X-ray crystallography, insights into the equilibrium distribution of these states and their kinetics have been provided by single-molecule florescence resonance energy transfer (smFRET) imaging[14] and double electron−electron resonance (DEER) spectroscopy measurements.[15]

The LeuT fold is shared by many transporters belonging to the NSS family, including Mhp1, vSGLT, BetP, CaiT, and AdiC1. Among them, dopamine transporter (DAT) controls dopamine levels in the synapse by cotransport of dopamine and two Na^+ ions and channeling of one chloride (Cl^-) ion. Dysfunction of human DAT (hDAT) has been linked to ADHD, bipolar disorder, clinical depression, and alcoholism.[16,17] DAT is a target for therapeutic antidepressants and for illicit or addictive drugs including cocaine and amphetamine (AMPH).[16−18] The first structure resolved for DAT was that of *Drosophila melanogaster* DAT (dDAT) in an antidepressant-bound OFo state,[19] and subsequently dopamine-, AMPH-, and cocaine-bound OF states have been resolved.[20] Human DAT (hDAT) shares more than 50% sequence identity with dDAT and 22% sequence identity with LeuT. We recently generated a structural model for the OFo hDAT monomer based on the known structure of the dDAT monomer; and showed that the

structure efficiently translocated dopamine from the EC to the IC region.[21]

At present, there is no consensus on whether the functional state of LeuT is monomeric or dimeric, or possibly both. Crystal structures in either homodimeric or monomeric state have been resolved for OF LeuT,[12,13,22] whereas the IFo structure has been resolved as a monomer.[12] The Gouaux lab investigated the LeuT structure in a range of crystal environments and reported that a frequent feature is the stabilization of a parallel LeuT dimer.[22] Moreover, oligomerization of NSSs has been suggested to be essential to their trafficking to the plasma membrane and efficient substrate transport.[23] DAT has been shown to exist as a dimer or a higher oligomer in several studies.[24−28] Oligomerization has been linked to cooperativity among monomeric units[29] and to AMPH-induced dopamine efflux.[30,31] The interfacial contacts observed in LeuT dimer are mainly between TM9 and TM12 (Figure 1A and B). In DAT, homodimers were detected upon cross-linking the EC ends of the TM6 helices using the endogenous Cys306.[24] In addition, a leucine repeat in TM2 of hDAT was implicated in oligomer formation[28] raising the question of whether NSS members could use different interfaces for oligomerization.

A number of computational studies have been performed for gaining further insights into the structure and dynamics of LeuT,[32−40] and hDAT using LeuT[41,42] or dDAT[21,43−45] as a template. Among them, our previous studies[39,40] were (to the best of our knowledge) the only simulations of LeuT wild-type (WT) dimer dynamics. The IFo dimer conformation was generated therein using the dimerization interface observed in the OFo crystal structure as a template. Likewise, using accelerated MD (aMD)[46] and conventional MD (cMD) we identified *in silico* the OFo and IFo conformations for hDAT
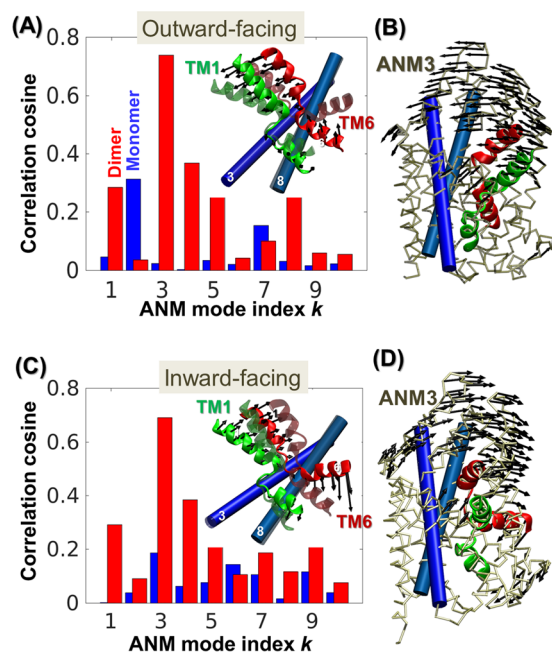
Figure 2. Overlap between computationally predicted ANM modes and experimentally observed structural change $d_{OF \leftrightarrow IF}$ for LeuT. (A and C) The bars display the correlation cosines between $d_{OF \leftrightarrow IF}$ and the ANM global modes 1−10 predicted for (A) OFo and (C) IFo conformers. Results for the LeuT dimer (residues R11-R507 of both protomers) and for the monomer (R11-R507) are shown by the respective red and blue bars. Protomers (red) exhibit a significantly higher overlap (than the isolated monomers) with experimental data. (B and D) Ribbon diagrams illustrate the movements along ANM mode 3 (ANM3) in both cases, which yields the highest overlap with experiments. Arrows indicate the directions of displacements; their lengths are based on an RMSD of 4 Å. For clarity, arrows shorter than 2.5 Å are not shown. The insets in (A) and (C) highlight the motions of TM1 (green) and TM6 (red). In this case, all arrows larger than 1 Å are shown. The starting and ending states of the helices are displayed in lighter/brighter and darker colors, respectively.

monomer,[21] and we generated structural models for the OFo and IFo hDAT dimers (unpublished results) by combining the results from docking and further MD simulations.

MD simulations can sample conformational states and transitions at atomic level. However, accurate sampling of the entire conformational space is a challenge, especially for large systems; and the cooperative dynamics of multimeric structures is often beyond the scope of MD simulations. To assess the functional significance of NSS oligomerization, at least from one perspective, we investigated the structural dynamics of LeuT and hDAT in both monomeric and dimeric forms using the anisotropic network model (ANM).[47] ANM is a simple physics-based model that approximates proteins as a network of beads and springs. The structural dynamics predicted by the ANM is fully defined by inter-residue contact topology. Earlier studies have shown that the global modes predicted by the ANM are robust to variations in local structure and energetics, and they closely overlap with principal modes of motions observed in micro- to millisecond MD simulations.[48−51] Moreover, ANM-predicted motions generally agree with the structural changes experimentally observed upon ligand/ inhibitor binding,[52−54] hence the development of ANM-based methods for exploring conformational transitions between known end points.[55−60] We evaluated here the ANM modes intrinsically accessible to the isolated monomers and to the

monomers in the dimers (called protomers), and compared them to the experimentally observed structural change $d_{OF \leftrightarrow IF}$ between the IF and OF states. Strikingly, dimerization dramatically increases the overlap between the ANM modes and the experimentally observed functional changes in structure. This suggests that dimerization increases the predisposition of NSS family members to undergo the global structural change—broadly termed alternating access,[61] and more recently described as rocking bundle mechanism[62]— required for accomplishing their substrate transport.

■ THEORETICAL METHODS

System Preparation. Equilibrated OFo and IFo conformers for LeuT dimer, based on the respective PDB structures[12] 3TT1 and 3TT3, were taken from our recent study.[39] No dimeric structure has been resolved to date for IF LeuT dimer. However, comparison of LeuT crystal structures shows that the interfacial helices TM9 (K376-F395) and TM12 (V483-R507) undergo minimal movements, if any, between the OF and IF states. The dimeric IFo structure was therefore modeled by registering the helices TM9 and TM12 in the same conformation as the OFo dimer (see Figure 1A and B), and subjected to energy minimization and equilibration protocols described earlier.[40,39] Briefly, each dimer was embedded in a 1-palmitoyl-2-oleoyl-phosphatidylethanolamine (POPE) membrane bilayer of size 155 × 110 × 53 Å^3 surrounded by a 150 mM NaCl aqueous solution, with at least 19 Å of lipid padding along the x/y axes and 18 Å of water along the z-axis. TIP3P water molecules and POPE head groups were modeled explicitly, whereas united-atom model was used for the POPE acyl chains.[63] All simulations were performed using NAMD-2.8[64] with CHARMM36 force field for lipids and proteins and the CMAP correction.[65] Structures were equilibrated with harmonic constraints on the protein backbone and substrate/ Na$^+$ atoms using force constants of 10 and 4 kcal.mol^{-1} Å^{-2} for the first 10 and following 20 ns, respectively. After equilibration, residue substitutions were performed to construct the WT LeuT; and a second energy minimization followed by 20 ns MD run was performed, with a force constant of 2 kcal.mol^{-1} Å^{-2}. Finally, cMD simulations were performed for 20 ns for further relaxation.

For constructing the hDAT dimer, we used the conformers sampled in our recent multimicroseconds aMD simulations of hDAT.[21] Conformers subjected to 2−10 ns cMD equilibration before transitioning into the OFc state were used as representative of the OFo state of the monomer; and the IF conformers temporarily stabilized after dopamine release were selected for representing the monomeric IFo state. These were used to construct models for hDAT dimer using the dimer docking module of Cluspro.[67] For each docking run, up to 30 best-scoring models were generated, which were then sorted based on four criteria: (1) stabilization of a symmetric or pseudosymmetric conformation; (2) positioning of the N- and C- termini to face the IC region; (3) proper orientation of aromatic residues (i.e., tryptophan) on the EC and IC sides to enable the anchoring to the lipid bilayer; and (4) preservation of interfacial contacts in different conformational states. These requirements were met by a few models only, the alignment of which is presented in Figure S1A (OFo dimer) and Figure S1B (IFo dimer). Both sets of models robustly shared the same type of interhelical contacts at their monomer−monomer interface. The root-mean-square deviation (RMSD) between any pair of dimeric conformers is smaller than 2.0 Å for OFo dimers, and

4.5 Å for IFo dimers. A representative conformer from each set (which showed the lowest RMSD with respect to all others) was selected for further refinement. The representative conformer was first placed in pre-equilibrated POPC and fully equilibrated TIP3 waters in a box of size $140 \times 140 \times 100$ Å³; energy-minimized for 50 000 step, followed by 0.5 ns runs at constant volume and temperature ($T = 310$ K) (NVT) and subsequent 4 ns runs at Nosé−Hoover constant pressure and temperature (1 bar, 310 K) (NPT), during which the protein was fixed, and the constraints on POPC head groups were gradually released. Then, the constraints on the protein backbone were released (from 10 kcal/mol to zero) within 3 ns. Finally, the unconstrained hDAT dimers were subjected to NPT simulations of 100 ns.

Closer examination of the monomeric structures in the IFo and OFo dimers, presented in Figure 1C,D, shows significant differences in the orientation of their TM1a-b, TM6a, and TM10 helices, consistent with the structural characteristics of the monomeric structures (see also Figure S1C). The dimerization interface is supported by two lines of experimental evidence (not used in model): (1) the Javitch group[24] showed that the hDAT dimer could form disulfide bridges between the Cys306 residues at the TM6 segment of each monomer; and (2) Torres et al.[28] proposed that the TM2 segment contributed to interfacial interactions in the hDAT dimer.

Anisotropic Network Model and Comparison with Experiments. In the ANM,[47] harmonic potentials of uniform force constants γ are adopted for all residue pairs within an interaction cutoff distance r_c, such that the total potential for a network of N residues is

$$V_{\text{ANM}} = -\gamma \left[\sum_{i=1}^{N-1} \sum_{j=i+1}^{N} (R_{ij} - R_{ij}^o)^2 \Gamma_{ij} \right] \tag{1}$$

Here, R_{ij} and R_{ij}^o are the instantaneous and original distances between the ith and j^{th} C^α-atoms. Γ is the Kirchhoff matrix, whose ij^{th} element, Γ_{ij}, is equal to -1 if $R_{ij}^o < r_c$ and $\Gamma_{ij} = 0$ otherwise; r_c is taken as 15 Å. V_{ANM} lends itself to a concise expression in terms of the components x_{ij}, y_{ij}, and z_{ij} of R_{ij}^o for the Hessian H_{ANM}, a symmetric $3N \times 3N$ matrix composed of 3 $\times$ 3 blocks H_{ij} of the form

$$H_{ij} = \frac{\gamma}{R_{ij}^{o2}} \begin{bmatrix} x_{ij}^2 & x_{ij}y_{ij} & x_{ij}z_{ij} \\ y_{ij}x_{ij} & y_{ij}^2 & y_{ij}z_{ij} \\ z_{ij}x_{ij} & z_{ij}y_{ij} & z_{ij}^2 \end{bmatrix} \tag{2}$$

for $i \neq j$, and the diagonal blocks are found from the negative sum of off-diagonal blocks on the same row (or column). eigenvalue decomposition of H_{ANM} yields $3N-6$ nonzero eigenvalues ($\lambda_1 \leq \lambda_2 \leq \cdots < \lambda_{3N-6}$). The eigenvector $u_k^T = [u_k^{X1}, u_k^{Y1}, u_k^{Z1}, \ldots u_k^{ZN}]$ (for $1 \leq k \leq 3N-6$) describes the normalized displacements of the N residues in 3D, driven by the kth mode. ANM modes can be readily evaluated using the ANM server.[68]

To compare the ANM-predicted modes of motion with experimental data, first we define the unit directional vector, $d_{\text{OF}\leftrightarrow\text{IF}}$, that describes the conformational difference between the two (experimentally known) end states of the examined structure. We focus here on global structural changes (OF↔IF), hence the omission of suffix o, in IFo or OFo states, which refers to local conformations of gating residues. $d_{\text{OF}\leftrightarrow\text{IF}}$ is given by

$$d_{\text{OF}\leftrightarrow\text{IF}} = (R^{\text{OF}} - R^{\text{IF}}) / \| R^{\text{OF}} - R^{\text{IF}} \| \tag{3}$$

where R^{OF} is the $3N$-dimensional conformational vector (of the coordinates of all C^α-atoms) in the OF state, and R^{IF} is that of the IF state, after optimal alignment of the two conformers. In the present case, the conformers were aligned by superposing their helices TM3 and TM8, which were practically unchanged between the two end points. The level of similarity between the ANM mode k accessible to OF state, $u_{k,\text{OF}}$, and the targeted transition OF → IF is measured by the overlap or correlation cosine[48]

$$O_{k,\text{OF}} = u_{k,\text{OF}} \cdot d_{\text{OF}\to\text{IF}} \tag{4}$$

and a similar expression holds for $O_{k,\text{IF}}$. $O_{k,\text{OF}}$ represents the fractional contribution of the kth mode (accessible to the OF state) to the change OF → IF. A high overlap achieved by a small set of soft modes (e.g., $k \leq 10$) indicates the predisposition of the structure to easily undergo these functional changes. We calculated the overlaps for (i) the individual monomers (in isolated state) and (ii) the protomers as part of the dimeric structures, using both the OF and IF states as initial conformers. Note that the $3N-6$ ANM modes form a complete orthonormal set of $3N$-dimensional basis vectors describing all possible directions of structural changes for the N residues in 3D space, such that cumulative overlap over m modes

$$\text{CO}_{m,\text{OF}} = \left[\sum_{k=1}^{m} (u_{k,\text{OF}} \cdot d_{\text{OF}\to\text{IF}})^2 \right]^{1/2} \tag{5}$$

sums up to 1 for m = 3N-6. A high cumulative overlap (e.g., > 0.80) obtained with a small number of soft modes (e.g., top 5−10) indicates the predisposition of the structure to undergo the reconfiguration $d_{\text{OF}\leftrightarrow\text{IF}}$[52−54] eqs 4 and 5 are directly adopted for the isolated monomers. For the protomers, on the other hand, we express $u_{k,\text{OF}}$ as $u_{k,\text{OF}}^T = [u_{A,k,\text{OF}}^T \ u_{B,k,\text{OF}}^T]$, where $u_{A,k,\text{OF}}$ represents the portion (one-half) of the eigenmode corresponding to protomer A, and superscript T denotes the transpose. Because this portion is not normalized, the overlap of individual modes with $d_{\text{OF}\leftrightarrow\text{IF}}$ is found from $O_{A,k}$ $= \left(\frac{u_{A,k,\text{OF}}^T}{|u_{A,k,\text{OF}}^T|} \cdot d_{\text{OF}\to\text{IF}} \right)$. $O_{A,k,\text{OF}}$ provides a quantitative measure of the propensity of protomer A to undergo the OF→IF transition based on the modes accessible to the protomer in the dimer. As to the evaluation of the cumulative overlap, we use in eq 5 the unit directional vectors along

$$u_{k,\text{OF}} = u_{A,k,\text{OF}} - \sum_{i=1}^{k-1} u_{A,k,\text{OF}} \cdot \frac{u_{A,i,\text{OF}}}{|u_{A,i,\text{OF}}|} \tag{6}$$

for $1 \leq k \leq 3N-6$. The second term in eq 6 ensures that the components of $u_{A,k,\text{OF}}$ used in the cumulative overlap are orthonormalized, and summation over all modes is identically equal to 1.

RESULTS AND DISCUSSION

LeuT: Dimerization Facilitates the Reconfiguration between OF and IF States. Our first goal was to examine to what extent the soft modes predicted by the ANM (at the lowest frequency end of the spectrum) concur with the experimentally observed structural change $d_{\text{OF}\leftrightarrow\text{IF}}$ between the IF and OF end states. Figure 2A and C display the overlaps between the modes, u_k, predicted by the ANM ($1 \leq k \leq 10$)
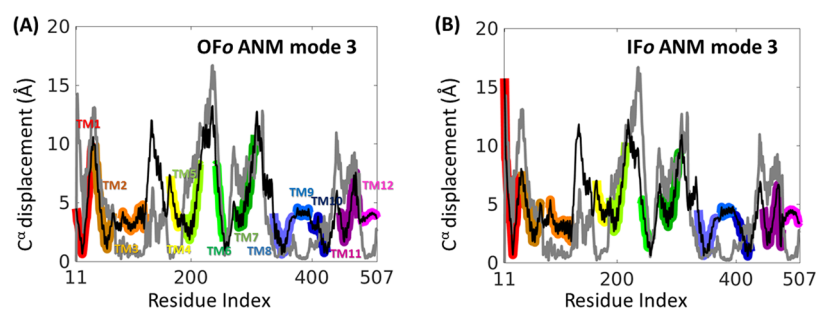
Figure 3. Comparison of residue displacements predicted by ANM mode 3 and that observed between two known conformations (OF and IF) of LeuT. The change in C^α-coordinates between OFo and IFo forms (gray thick curve), and the ANM3-driven distribution of residue motions (black) for the OFo state (A) and the IFo state (B) are shown. The absolute values are obtained by uniformly rescaling the profile to match the norm of the displacement vector $d_{\text{OF}\leftrightarrow\text{IF}}$. TM helices are highlighted in colors in accord with those in Figure 1.
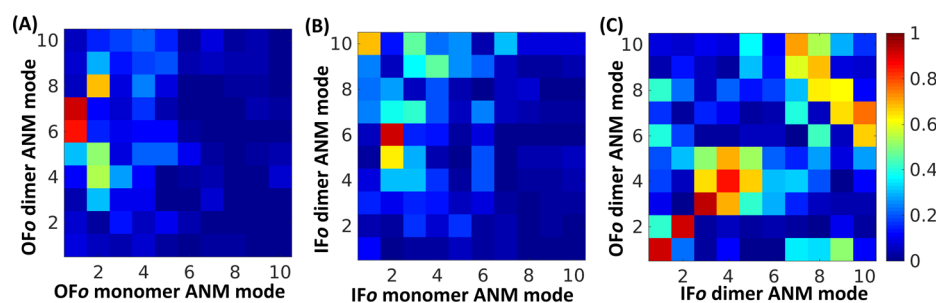

Figure 4. Correlations between the modes accessible to the isolated monomer and the protomers in the dimer. Shown here are the correlation cosines of the first 10 ANM modes of the (A) OFo monomer (abscissa) and OFo protomer in the dimer (ordinate), (B) IFo monomer (abcissa) and IFo protomer in the dimer (ordinate), and (C) protomers in IFo dimer (abscissa) and OFo dimer (ordinate). The correlation cosines for the protomers were calculated by taking half of the dimeric ANM modes (for one protomer) and then normalizing them to become unit vectors.

and $d_{\text{OF}\leftrightarrow\text{IF}}$. ANM modes were computed for the OF (A) or the IF (C) conformer (as initial structure), and the overlaps are reported for the TM helical domains as the main determinants of the OF and IF states. Two sets of results are presented in each panel: (i) for the isolated monomers (blue bars), and (ii) for the protomers in the dimeric structures (red bars). The modes predicted for the monomers exhibit modest overlaps with experiments, with the highest value obtained for ANM mode 2 (ANM2) of the OF monomer (A). In contrast, the ANM modes for the protomers show significantly higher overlaps with the experimentally observed structural change. Thus, dimerization enhances the ability of the monomers to undergo soft modes that are in remarkable agreement with the functional change in structure sampled during the transport cycle. In particular, ANM3 for the OF dimer yields an overlap of 0.74; and ANM3 for IF dimer, 0.69. The collective movements along these modes are illustrated in Figure 2B and D for the respective OFo and IFo dimers. It is remarkable to see that a single mode, out of 3N-6 accessible to the dimeric structure, can help achieve about 70% of the change required to transition from OF to IF state. Therefore, the protomers in the dimers are strongly predisposed to undergo the transition between the OF and IF states, while this tendency is weaker in the monomeric state.

The softest mode that favors the functional transition of LeuT protomer is closely shared between the OF and IF dimers. Figure 3 compares the residue displacements along the mode 3 (ANM3) and those taking place during the OFo ↔ IFo transition, for the OFo (A) or the IFo (B) conformers. ANM3 in either case practically shows the same features, and may be viewed as the opposite direction fluctuations of the same soft mode shared by the two end points. As can be seen in the insets

in panels A and C of Figure 2 as well as panels B and D, the most outstanding feature of this mode is the reorientations of the C-terminal half of TM1 (TM1b) and N-terminal half of TM6 (TM6a) with respect to TM3 and TM8, in line with the opening/closing of the EC thick gate (Krishnamurthy et al.[12] provide a detailed description of the EC gate). In the OF state, ANM3 contributes to the opening of the IC vestibule by rotating TM1a and 6b, and in the IF state, it drives the closure of the same vestibule. In addition, in the OFo state, the same mode drives the concerted movements of the helices TM2, 5, 7, and 11 toward their IFo coordinates. ANM3 of the IFo, on the other hand, drives the reverse movements.

A closer look reveals that the soft modes that predominantly enable the OF ↔IF transition are unique to dimeric state; they are acquired upon dimerization. We further examined to what extent the intrinsic motions accessible to the isolated monomers are retained in the dimer. The correlation maps in Figure 4A,B display the correlation cosines between the ANM modes for the monomer and those for the protomer in the dimer. We note that the ANM modes that facilitate the transition between the IF and OF states are acquired in the dimeric state only. ANM mode 3 is hardly observable in the monomer. Dimerization appears to add 2 or 3 new global modes of motion to the lowest frequency end of the spectrum (bottom rows in maps A and B). The same feature can be discerned in the eigenvalue spectra presented in Figure S2. Dimeric structures have access to a larger number of low frequency modes (i.e., the slowest modes of the dimers entail lower frequency movements compared to the monomers). A handful of soft modes accessible to the dimer reach a cumulative overlap of more than 0.80 with the structural change between the IF and OF forms, which is much higher
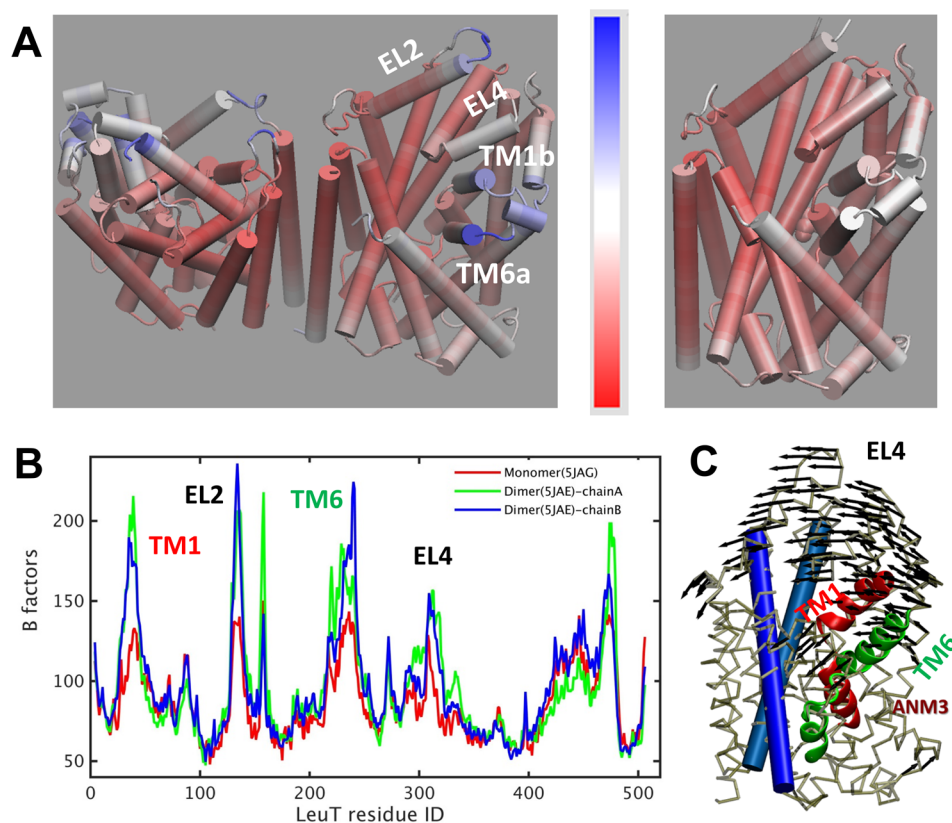
Figure 5. Comparison of B-factors in LeuT dimer and monomer. (A) The crystal structures of LeuT dimer (PDB: 5JAE) and T354H mutant monomer (PDB: 5JAG) in the outward-facing sodium free state.[13] The B-factors are color-coded using the same scale from low (red) to high (blue) values. (B) Comparison of the B-factors in the monomer and two different subunits in the dimer (left panel). TM1, TM6, EL2, and EL4 exhibit an enhanced mobility in the dimer, consistent with the predicted mode 3 for the dimers. Panel C is reproduced from here from Figure 2B to ease the comparison.

than those of the monomer. Supplementary Figures S3 and S4 compare the cumulative overlap plots for the monomers (blue squares) and protomers (red dots), evaluated for the OF (Figure S3) and IF (Figure S4) structures. Notably the softest three modes alone accessible to the protomers achieve a cumulative of ≥0.75 in both cases, whereas the corresponding overlaps for the monomers remain ≤0.30.

Comparison of ANM modes predicted for the OF*o* and IF*o* dimers (Figure 4C) shows that the two dimeric structures (OF and IF) robustly select highly similar soft modes, which provide a direct conduit for their interconversion. ANM3 predicted for OF*o* dimer shows a correlation cosine of 0.93 with ANM3 of IF*o* dimer. The comparison of the overlaps (with $d_{OF↔IF}$) achieved by the individual modes accessible to the OF*o* and IF*o* dimers illustrated in Figure 2 and Figure S5 further discloses the close similarity between the soft modes favored by either dimer.

Taken together, we found that dimerization of LeuT alters the intrinsic dynamics accessible to the protomers toward favoring the functional transitions (OF ↔ IF) (Figures 1–4). In particular, an enhancement in the mobility of TM helices TM1 and TM6, and the EC-exposed loops EL2 and EL4 is observed in the dimer (Figure 2B).

The effect of dimerization on the equilibrium fluctuations of monomers can be detected in the B-factors reported in the recent crystallographic study of Nissen and co-workers,[13] shown in Figure 5. Comparison of the B-factors reported for the isolated monomers and those in the dimer shows that dimerization induces an enhanced mobility in TM1 and TM6

helices, and in EL2 and EL4 loops in both subunits. These coincide with the regions shown by the ANM3 to exhibit increased mobility in favor of the transition from the OF to IF state.

hDAT: Dimerization Facilitates hDAT Transitions between OF and IF States. ANM analysis performed for hDAT monomers and dimers in their IF*o* and OF*o* states essentially yielded the same qualitative features as those obtained for LeuT. Figures 6–8 below for hDAT are the counterparts of Figures 2–4 for LeuT, and Supplementary Figures S6–S9 (for hDAT) are the counterparts of Figures S2–S5 (for LeuT). Dimerization has again a significant contribution to enhancing the propensity of the protomers to undergo the functional OF↔IF transition, as shown in Figure 6A,B. ANM mode 3 obtained for the OF*o* dimer is illustrated in Figure 6C. The $C^α$-displacements driven by these modes are plotted in Figure 7A against the change in residue positions described by $d_{OF↔IF}$. The close agreement confirms that this mode favored by the dimer architecture facilitates the transition of the protomers from OF state into IF*o* conformer. The most outstanding feature of ANM3 is the rearrangement of TM2, 5–7, 10, and 12 toward their respective IF*o* coordinates. ANM3 also contributes to the reorientation of TM1b and TM6a, essential to closing the EC vestibule, and to opening of the IC vestibule by rotating TM1a. ANM4 obtained for hDAT IF*o* dimer, on the other hand, is illustrated in Figure 7B. ANM4 reorients TM1 in such a manner that the EC vestibule opens and the IC vestibule closes. In addition, it repositions TM2 and 10 toward their conformations in the OF*o* state.
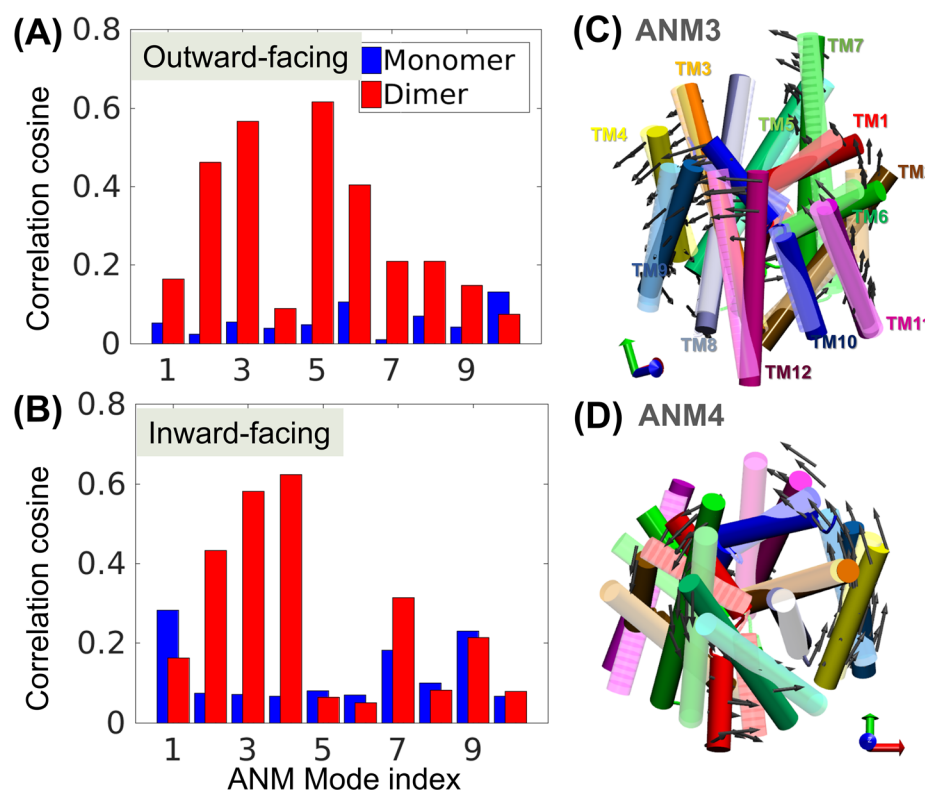
Figure 6. Overlap between ANM modes and the structural change $d(\text{OF}o \leftrightarrow \text{IF}o)$ for hDAT, and dominant modes that contribute to the transition. (A,B) The bars display the correlation cosines between $d(\text{OF}o \leftrightarrow \text{IF}o)$ and the ANM modes predicted for (A) OF and (B) IF states. Results for the protomers in hDAT dimer and the isolated monomers are shown by the respective red and blue bars. The ANM analysis for hDAT included the complete structures. For overlap calculations, all TM helices (TM1a, 1b, TM2-TM12), the IC helix IL5, and the EC loops EL2, EL3, and EL4a and b were used. (C,D) ANM modes that yielded high overlaps with $d(\text{OF}o \leftrightarrow \text{IF}o)$. Arrows indicate the displacements based on an RMSD of 5 Å in each mode. For clarity only arrows larger than 2.5 Å are shown.
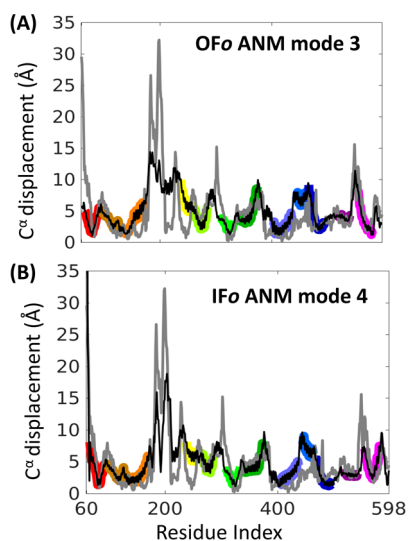

Figure 7. Comparison of the residue displacements driven by selected ANM modes and those observed between the OF and IF states of hDAT. The changes in C^α-coordinates between OFo and IFo states (gray), and the predicted distribution of motions (black) are shown for (A) OFo structure, ANM mode 3, and (B) IFo structure ANM mode 4. TM helices are colored as in Figure 6.

The cross-correlations between the ANM modes accessible to protomers within the dimers, and those accessible to the isolated monomers are presented in Figure 8A,B. The modes that facilitate the transition (ANM modes 1−3 and 5) are not present in the hDAT monomer. Similarly, for the IFo state no counterpart for ANM1−3 of the dimer exists in the mode spectrum of the monomer. However, ANM4 of IF protomer shows an overlap of 0.64 with ANM1 of IFo monomer. The latter yields an overlap of 0.28 with the IF$o \rightarrow$ OFo transition (Figure S8). Thus, dimerization improves this intrinsic ability of the monomer in addition to endowing new modes. Figure 8C shows the similarity between ANM modes in the OFo and IFo states. The overlaps between OFo ANM3 and IFo ANM4 is 0.87, again indicating that the modes favoring the reconfiguration along OF↔IF are conserved among the two end states.

CONCLUSION

In this study, we investigated the effect of dimerization on LeuT and hDAT structural dynamics using the ANM. ANM analysis has been applied to the monomeric and dimeric forms of two transporters that share the same fold: LeuT and DAT. The results highlight the significance of dimerization for promoting the transitions between the outward- and inward-facing states of either transporter. In the monomeric state, the intrinsic collective motions could account only for a moderate portion of the transition. Strikingly, in dimeric state, ANM-predicted soft modes were found to yield correlation cosines 0.60 to 0.70 with the global change OF$o \leftrightarrow$ IFo. This is a remarkable result, as it indicates that dimerization favors the functional transition of each unit, which also suggests that those transporters in the dimeric state are likely to transport their substrate more efficiently than what would be expected from the sum of individual monomers.
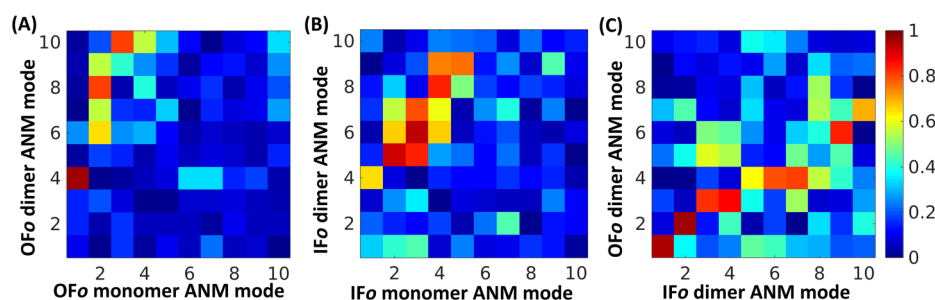
Figure 8. Correlations between ANM modes computed for protomers in dimers and isolated monomers, starting from OF*o* and IF*o* forms. The correlation cosines between the first 10 ANM modes of (A) a protomer in the OF*o* dimer (ordinate) and OF*o* monomer (abscissa), (B) IF*o* protomer in dimer (ordinate) and IF*o* monomer (abscissa), and (C) protomers belonging to IF*o* dimer (ordinate) and OF*o* dimer (abscissa).

It is important to note that the modes of motions that favor the transition rank among the softest modes (which are most accessible energetically). The significant overlap between these modes (in the dimeric state) and the conformational transitions that take place during the transport cycle suggests that dimerization may be an enhancing factor, if not a requirement, for achieving biological function in the NSS family of transporters. A major effect of dimerization is to stabilize the interfacial regions (TM9 and 12 in LeuT, and TM11, TM2, and TM6 in hDAT), while enhancing the movements of TM1, TM6, EL2, and EL4. Notably, comparison of the fluctuation spectra of monomeric and dimeric LeuT crystals indicated the same type of changes in the mobilities of individual segments upon dimerization (Figure 5).

Another interesting result was to see that the modes of motion that facilitated the transition were closely conserved between OF and IF states. OF*o* LeuT dimer ANM mode 3, which yielded an overlap of 0.74 with the OF*o* → IF*o* deformation vector, was also favored by the IF*o* LeuT dimer, with a correlation cosine of 0.93. A similar behavior was observed for hDAT dimer. The two modes of the OF*o* dimer, ANM3 and 5, which were found to closely agree with the functional transition, were highly similar to IF*o* modes ANM3 and 4. Overall our study provides one more evidence for the evolution of structures to intrinsically favor motions that are functional, as suggested earlier.[69] However, the striking result here is that, not only native inter-residue contact topologies of proteins, but also their oligomerization geometry has evolved to favor functional changes in structure.

In the current study, the predisposition to undergo a change, rather than the complete transition pathway, has been examined. There are several studies, including our own based on the ANM for exploring the transition paths between known end states,[55−60] which provide rough estimates on energy barriers (in arbitrary units). For example, we recently investigated the LeuT energy based on 21 μs of MD simulations of the dimer,[39] and we have examined the transition pathway of LeuT monomer using the ANM pathway methodology.[54] We and others have also reported that the hydration of the Na2 site facilitates the conformational transition of hDAT from the OF to IF state.[21,44,45] In particular, the interaction of the N-terminus with PIP$_2$ lipids was reported to induce spontaneous inward opening of hDAT.[44] The present study does not incorporate the effect of hydration, nor interactions with lipids; it focuses on the intrinsic "directions" or the softest movements accessible near the starting energy minimum. The results are robust and physically plausible, given that the linear approximation underlying elastic network models is strictly valid near energy minima.

The accessibility of the same mechanism of motion in opposite directions (e.g., ANM3 of OF and IF LeuT dimer) suggests that these modes may provide a conduit for the complete passage between these end points. We refrain however from speculating on detailed/complete transition pathway(s) and limit our analysis to clearly favored softest modes in the vicinity of the starting conformer. The cumulative overlaps demonstrate that completion of the transition requires the addition of higher frequency (stiffer) modes, or even an adaptive reevaluation of the mode spectra if local minima are visited. However, the dispersion of the modes also clearly demonstrates that the top-ranking modes that assist in the reconfiguration of the protomers along the targeted direction $d_{\mathrm{OF}\leftrightarrow\mathrm{IF}}$ are acquired in the dimeric state, and that they are softer (have smaller eigenvalue/frequency) than the softest modes accessible to the monomer. This analysis suggests that dimerization enhances the motility of some domains, and that the increased motions of those domains are in a direction similar to that required to undergo the OF ↔ IF transition.

Finally, the method of approach presented here for LeuT and hDAT is straightforward, and can be reproduced using our ANM server,[68] and adopted to comparing the predisposition of subunits in multimeric structures or complexes to undergo known transitions, compared to their ability to do so in the monomeric/uncomplexed state. This type of analysis may provide new insights into the gain or loss in biomolecular function induced multimeric assembly or complexation.

■ ASSOCIATED CONTENT

Ⓢ Supporting Information

The Supporting Information is available free of charge on the ACS Publications website at DOI: 10.1021/acs.jpcb.6b09876.

Alignment of computed hDAT dimer models; distribution of eigenvalues for LeuT structures in the dimeric and monomeric forms, shown for outward-facing (OF) and inward-facing (IF) states; cumulative overlaps between OF*o* ANM modes and the structural change $d(\mathrm{OF}o \leftrightarrow \mathrm{IF}o)$ for LeuT; cumulative overlaps between IF*o* ANM modes and the structural change $d(\mathrm{OF}o \leftrightarrow \mathrm{IF}o)$ for LeuT; overlap between orthonormalized ANM modes and experimentally observed structural change $d_{\mathrm{OF}\leftrightarrow\mathrm{IF}}$ for LeuT; distribution of eigenvalues for hDAT dimers and monomers, shown for outward-facing (OF) and inward-facing (IF) states; cumulative overlaps between OF*o* ANM modes and the structural change $d(\mathrm{OF}o \leftrightarrow \mathrm{IF}o)$ for hDAT; cumulative overlaps between

IFo ANM modes and the structural change $d($OF$o \leftrightarrow$ IF$o)$ for hDAT; and overlap between orthonormalized ANM modes and structural change $d_{\text{OF} \leftrightarrow \text{IF}}$ for hDAT (PDF)

■ AUTHOR INFORMATION

Corresponding Authors

*Telephone: +90 212 293 13 00; Fax: +90 212 245 07 95; E-mail: gurme@itu.edu.tr.

*Telephone: +1 412 648 3332; Fax: +1 412 648 3163; E-mail: bahar@pitt.edu.

ORCID ⊙

Mert Gur: 0000-0003-0983-4397

Notes

The authors declare no competing financial interest.

■ REFERENCES

(1) Jessell, T. M.; Kandel, E. R. Synaptic transmission: a bidirectional and self-modifiable form of cell-cell communication. *Cell* **1993**, *72* (Suppl), 1−30.

(2) Amara, S. G.; Kuhar, M. J. Neurotransmitter transporters: recent progress. *Annu. Rev. Neurosci.* **1993**, *16*, 73−93.

(3) Iversen, L. L.; Kelly, J. S. Uptake and metabolism of gamma-aminobutyric acid by neurones and glial cells. *Biochem. Pharmacol.* **1975**, *24*, 933−938.

(4) Rudnick, G. Ion-coupled neurotransmitter transport: thermodynamic vs. kinetic determinations of stoichiometry. *Methods Enzymol.* **1998**, *296*, 233−247.

(5) Richerson, G. B.; Wu, Y. Role of the GABA transporter in epilepsy. *Adv. Exp. Med. Biol.* **2004**, *548*, 76−91.

(6) Andersen, J.; Kristensen, A. S.; Bang-Andersen, B.; Stromgaard, K. Recent advances in the understanding of the interaction of antidepressant drugs with serotonin and norepinephrine transporters. *Chem. Commun. (Cambridge, U. K.)* **2009**, *25*, 3677−3692.

(7) Schafer, W. R. How do antidepressants work? Prospects for genetic analysis of drug mechanisms. *Cell* **1999**, *98*, 551−554.

(8) Hahn, M. K.; Blakely, R. D. Monoamine transporter gene structure and polymorphisms in relation to psychiatric and other complex disorders. *Pharmacogenomics J.* **2002**, *2*, 217−235.

(9) Clausen, R. P.; Madsen, K.; Larsson, O. M.; Frolund, B.; Krogsgaard-Larsen, P.; Schousboe, A. Structure-activity relationship and pharmacology of gamma-aminobutyric acid(GABA) transport inhibitors. *Adv. Pharmacol.* **2006**, *54*, 265−284.

(10) Waldman, I. D.; Rowe, D. C.; Abramowitz, A.; Kozel, S. T.; Mohr, J. H.; Sherman, S. L.; Cleveland, H. H.; Sanders, M. L.; Gard, J. M.; Stever, C. Association and linkage of the dopamine transporter gene and attention-deficit hyperactivity disorder in children: heterogeneity owing to diagnostic subtype and severity. *Am. J. Hum. Genet.* **1998**, *63*, 1767−1776.

(11) Yamashita, A.; Singh, S. K.; Kawate, T.; Jin, Y.; Gouaux, E. Crystal structure of a bacterial homologue of Na$^+$/Cl$^-$ dependent neurotransmitter transporters. *Nature* **2005**, *437*, 215−223.

(12) Krishnamurthy, H.; Gouaux, E. X-ray structures of LeuT in substrate-free outward-open and apo inward-open states. *Nature* **2012**, *481*, 469−474.

(13) Malinauskaite, L.; Said, S.; Sahin, C.; Grouleff, J.; Shahsavar, A.; Bjerregaard, H.; Noer, P.; Severinsen, K.; Boesen, T.; Schiott, B.; et al. A conserved leucine occupies the empty substrate site of LeuT in the Na$^+$-free return state. *Nat. Commun.* **2016**, *7*, 11673.

(14) Zhao, Y.; Terry, D.; Shi, L.; Weinstein, H.; Blanchard, S. C.; Javitch, J. A. Single-molecule dynamics of gating in a neurotransmitter transporter homologue. *Nature* **2010**, *465*, 188−193.

(15) Kazmier, K.; Sharma, S.; Quick, M.; Islam, S. M.; Roux, B.; Weinstein, H.; Javitch, J. A.; Mchaourab, H. S. Conformational dynamics of ligand-dependent alternating access in LeuT. *Nat. Struct. Mol. Biol.* **2014**, *21*, 472−479.

(16) Reith, M. *Neurotransmitter transporters: structure, function, and regulation*; Springer Science & Business Media, 2002.

(17) Vaughan, R. A.; Foster, J. D. Mechanisms of dopamine transporter regulation in normal and disease states. *Trends Pharmacol. Sci.* **2013**, *34*, 489−496.

(18) Amara, S. G.; Sonders, M. S. Neurotransmitter transporters as molecular targets for addictive drugs. *Drug Alcohol Depend.* **1998**, *51*, 87−96.

(19) Penmatsa, A.; Wang, K. H.; Gouaux, E. X-ray structure of dopamine transporter elucidates antidepressant mechanism. *Nature* **2013**, *503*, 85−90.

(20) Wang, K. H.; Penmatsa, A.; Gouaux, E. Neurotransmitter and psychostimulant recognition by the dopamine transporter. *Nature* **2015**, *521*, 322−327.

(21) Cheng, M. H.; Bahar, I. Molecular mechanism of dopamine transport by human dopamine transporter. *Structure* **2015**, *23*, 2171−2181.

(22) Wang, H.; Elferich, J.; Gouaux, E. Structures of LeuT in bicelles define conformation and substrate binding in a membrane-like context. *Nat. Struct. Mol. Biol.* **2012**, *19*, 212−219.

(23) Sorkina, T.; Doolen, S.; Galperin, E.; Zahniser, N. R.; Sorkin, A. Oligomerization of dopamine transporters visualized in living cells by fluorescence resonance energy transfer microscopy. *J. Biol. Chem.* **2003**, *278*, 28274−28283.

(24) Hastrup, H.; Karlin, A.; Javitch, J. A. Symmetrical dimer of the human dopamine transporter revealed by cross-linking Cys-306 at the extracellular end of the sixth transmembrane segment. *Proc. Natl. Acad. Sci. U. S. A.* **2001**, *98*, 10055−10060.

(25) Hastrup, H.; Sen, N.; Javitch, J. A. The human dopamine transporter forms a tetramer in the plasma membrane: cross-linking of a cysteine in the fourth transmembrane segment is sensitive to cocaine analogs. *J. Biol. Chem.* **2003**, *278*, 45045−45048.

(26) Li, Y.; Cheng, S. Y.; Chen, N.; Reith, M. E. Interrelation of dopamine transporter oligomerization and surface presence as studied with mutant transporter proteins and amphetamine. *J. Neurochem.* **2010**, *114*, 873−885.

(27) Sitte, H. H.; Farhan, H.; Javitch, J. A. Sodium-dependent neurotransmitter transporters: oligomerization as a determinant of transporter function and trafficking. *Mol. Interventions* **2004**, *4*, 38−47.

(28) Torres, G. E.; Carneiro, A.; Seamans, K.; Fiorentini, C.; Sweeney, A.; Yao, W. D.; Caron, M. G. Oligomerization and trafficking of the human dopamine transporter. Mutational analysis identifies critical domains important for the functional expression of the transporter. *J. Biol. Chem.* **2003**, *278*, 2731−2739.

(29) Zhen, J.; Antonio, T.; Cheng, S. Y.; Ali, S.; Jones, K. T.; Reith, M. E. Dopamine transporter oligomerization: impact of combining protomers with differential cocaine analog binding affinities. *J. Neurochem.* **2015**, *133*, 167−173.

(30) Sitte, H. H.; Schutz, G. J.; Freissmuth, M. Cooperativity between individual transporter protomers: new data fuelling old complexes. *J. Neurochem.* **2015**, *133*, 163−166.

(31) Sitte, H. H.; Freissmuth, M. Amphetamines, new psychoactive drugs and the monoamine transporter cycle. *Trends Pharmacol. Sci.* **2015**, *36*, 41−50.

(32) Shaikh, S. A.; Tajkhorshid, E. Modeling and dynamics of the inward-facing state of a Na$^+$/Cl$^-$ dependent neurotransmitter transporter homologue. *PLoS Comput. Biol.* **2010**, *6*, e1000905.

(33) Grouleff, J.; Sondergaard, S.; Koldso, H.; Schiott, B. Properties of an inward-facing state of LeuT: conformational stability and substrate release. *Biophys. J.* **2015**, *108*, 1390−1399.

(34) Celik, L.; Schiott, B.; Tajkhorshid, E. Substrate binding and formation of an occluded state in the leucine transporter. *Biophys. J.* **2008**, *94*, 1600−1612.

(35) Cheng, M. H.; Bahar, I. Coupled global and local changes direct substrate translocation by neurotransmitter-sodium symporter ortholog LeuT. *Biophys. J.* **2013**, *105*, 630−639.

(36) Cheng, M. H.; Bahar, I. Complete mapping of substrate translocation highlights the role of LeuT N-terminal segment in regulating transport cycle. *PLoS Comput. Biol.* **2014**, *10*, e1003879.

(37) Thomas, J. R.; Gedeon, P. C.; Grant, B. J.; Madura, J. D. LeuT conformational sampling utilizing accelerated molecular dynamics and principal component analysis. *Biophys. J.* **2012**, *103*, L1−L3.

(38) Shi, L.; Quick, M.; Zhao, Y.; Weinstein, H.; Javitch, J. A. The mechanism of a neurotransmitter:sodium symporter–inward release of Na$^+$ and substrate is triggered by substrate in a second binding site. *Mol. Cell* **2008**, *30*, 667−677.

(39) Gur, M.; Zomot, E.; Cheng, M. H.; Bahar, I. Energy landscape of LeuT from molecular simulations. *J. Chem. Phys.* **2015**, *143*, 243134.

(40) Zomot, E.; Gur, M.; Bahar, I. Microseconds simulations reveal a new sodium-binding site and the mechanism of sodium-coupled substrate uptake by LeuT. *J. Biol. Chem.* **2015**, *290*, 544−555.

(41) Indarte, M.; Madura, J. D.; Surratt, C. K. Dopamine transporter comparative molecular modeling and binding site prediction using the LeuT(Aa) leucine transporter as a template. *Proteins: Struct., Funct., Genet.* **2008**, *70*, 1033−1046.

(42) Beuming, T.; Kniazeff, J.; Bergmann, M. L.; Shi, L.; Gracia, L.; Raniszewska, K.; Newman, A. H.; Javitch, J. A.; Weinstein, H.; Gether.; et al. The binding sites for cocaine and dopamine in the dopamine transporter overlap. *Nat. Neurosci.* **2008**, *11*, 780−789.

(43) Cheng, M. H.; Block, E.; Hu, F.; Cobanoglu, M. C.; Sorkin, A.; Bahar, I. Insights into the Modulation of Dopamine Transporter Function by Amphetamine, Orphenadrine, and Cocaine Binding. *Front Neurol.* **2015**, *6*, 134.

(44) Khelashvili, G.; Stanley, N.; Sahai, M. A.; Medina, J.; LeVine, M. V.; Shi, L.; De Fabritiis, G.; Weinstein, H. Spontaneous inward opening of the dopamine transporter is triggered by PIP$_2$-regulated dynamics of the N-terminus. *ACS Chem. Neurosci.* **2015**, *6*, 1825−1837.

(45) Razavi, A. M.; Khelashvili, G.; Weinstein, H. A Markov state-based quantitative kinetic model of sodium release from the dopamine transporter. *Sci. Rep.* **2017**, *7*, 40076.

(46) Hamelberg, D.; Mongan, J.; McCammon, J. A. Accelerated molecular dynamics: a promising and efficient simulation method for biomolecules. *J. Chem. Phys.* **2004**, *120*, 11919−11929.

(47) Atilgan, A. R.; Durell, S. R.; Jernigan, R. L.; Demirel, M. C.; Keskin, O.; Bahar, I. Anisotropy of fluctuation dynamics of proteins with an elastic network model. *Biophys. J.* **2001**, *80*, 505−515.

(48) Gur, M.; Zomot, E.; Bahar, I. Global motions exhibited by proteins in micro- to milliseconds simulations concur with anisotropic network model predictions. *J. Chem. Phys.* **2013**, *139*, 121912.

(49) Leioatts, N.; Romo, T. D.; Grossfield, A. Elastic network models are robust to variations in formalism. *J. Chem. Theory Comput.* **2012**, *8*, 2424−2434.

(50) Romo, T. D.; Grossfield, A. Validating and improving elastic network models with molecular dynamics simulations. *Proteins: Struct., Funct., Genet.* **2011**, *79*, 23−34.

(51) Zheng, W.; Brooks, B. R.; Thirumalai, D. Low-frequency normal modes that describe allosteric transitions in biological nanomachines are robust to sequence variations. *Proc. Natl. Acad. Sci. U. S. A.* **2006**, *103*, 7664−7669.

(52) Meireles, L.; Gur, M.; Bakan, A.; Bahar, I. Pre-existing soft modes of motion uniquely defined by native contact topology facilitate ligand binding to proteins. *Protein Sci.* **2011**, *20*, 1645−1658.

(53) Bakan, A.; Bahar, I. The intrinsic dynamics of enzymes plays a dominant role in determining the structural changes induced upon inhibitor binding. *Proc. Natl. Acad. Sci. U. S. A.* **2009**, *106*, 14349−14354.

(54) Tobi, D.; Bahar, I. Structural changes involved in protein binding correlate with intrinsic motions of proteins in the unbound state. *Proc. Natl. Acad. Sci. U. S. A.* **2005**, *102*, 18908−18913.

(55) Das, A.; Gur, M.; Cheng, M. H.; Jo, S.; Bahar, I.; Roux, B. Exploring the conformational transitions of biomolecular systems using a simple two-state anisotropic network model. *PLoS Comput. Biol.* **2014**, *10*, e1003521.

(56) Gur, M.; Madura, J. D.; Bahar, I. Global transitions of proteins explored by a multiscale hybrid methodology: application to adenylate kinase. *Biophys. J.* **2013**, *105*, 1643−1652.

(57) Kim, M. K.; Jernigan, R. L.; Chirikjian, G. S. Efficient generation of feasible pathways for protein conformational transitions. *Biophys. J.* **2002**, *83*, 1620−1630.

(58) Kurkcuoglu, Z.; Bahar, I.; Doruker, P. ClustENM: ENM-based sampling of essential conformational space at full atomic resolution. *J. Chem. Theory Comput.* **2016**, *12*, 4549−4562.

(59) Seo, S.; Jang, Y.; Qian, P.; Liu, W. K.; Choi, J. B.; Lim, B. S.; Kim, M. K. Efficient prediction of protein conformational pathways based on the hybrid elastic network model. *J. Mol. Graphics Modell.* **2014**, *47*, 25−36.

(60) Isin, B.; Schulten, K.; Tajkhorshid, E.; Bahar, I. Mechanism of signal propagation upon retinal isomerization: Insights from molecular dynamics simulations of rhodopsin restrained by normal modes. *Biophys. J.* **2008**, *95*, 789−803.

(61) Jardetzky, O. Simple allosteric model for membrane pumps. *Nature* **1966**, *211*, 969−970.

(62) Forrest, L. R.; Rudnick, G. The rocking bundle: a mechanism for ion-coupled solute flux by symmetrical transporters. *Physiology* **2009**, *24*, 377−386.

(63) Hénin, J.; Shinoda, W.; Klein, M. L. United-atom acyl chains for CHARMM phospholipids. *J. Phys. Chem. B* **2008**, *112*, 7008−7015.

(64) Phillips, J. C.; Braun, R.; Wang, W.; Gumbart, J.; Tajkhorshid, E.; Villa, E.; Chipot, C.; Skeel, R. D.; Kale, L.; Schulten, K. Scalable molecular dynamics with NAMD. *J. Comput. Chem.* **2005**, *26*, 1781−1802.

(65) Mackerell, A. D., Jr.; Feig, M.; Brooks, C. L. 3. Extending the treatment of backbone energetics in protein force fields: limitations of gas-phase quantum mechanics in reproducing protein conformational distributions in molecular dynamics simulations. *J. Comput. Chem.* **2004**, *25*, 1400−1415.

(66) Humphrey, W.; Dalke, A.; Schulten, K. VMD: visual molecular dynamics. *J. Mol. Graphics* **1996**, *14*, 33−38.

(67) Comeau, S. R.; Gatchell, D. W.; Vajda, S.; Camacho, C. J. ClusPro: an automated docking and discrimination method for the prediction of protein complexes. *Bioinformatics* **2004**, *20*, 45−50.

(68) Eyal, E.; Lum, G.; Bahar, I. The anisotropic network model web server at 2015(ANM 2.0). *Bioinformatics* **2015**, *31*, 1487−1489.

(69) Haliloglu, T.; Bahar, I. Adaptability of protein structures to enable functional interactions and evolutionary implications. *Curr. Opin. Struct. Biol.* **2015**, *35*, 17−23.